# Semi-analytical solution for the dynamic response of a cylindrical structure embedded in a homogeneous half-space

Zhao, Mingjuan; van Dalen, Karel N.; Barbosa, João M.; Metrikine, Andrei V.

**DOI**
10.1007/978-981-10-4508-0_35

**Publication date**
2018

**Document Version**
Accepted author manuscript

**Published in**
Environmental Vibrations and Transportation Geodynamics

**Citation (APA)**
Zhao, M., van Dalen, K. N., Barbosa, J. M., & Metrikine, A. V. (2018). Semi-analytical solution for the dynamic response of a cylindrical structure embedded in a homogeneous half-space. In X. Bian, Y. Chen, & X. Ye (Eds.), *Environmental Vibrations and Transportation Geodynamics: ISEV 2016, Hangzhou China* (212039 ed., pp. 369-388). Springer. https://doi.org/10.1007/978-981-10-4508-0_35

# Semi-analytical solution for the dynamic response of a cylindrical structure embedded in a homogeneous half-space

Mingjuan Zhao, Karel N. van Dalen, João M. Barbosa, Andrei V. Metrikine
Department of Structural Engineering, Delft University of Technology, 2628 CN Delft, The Netherlands
M.Zhao@tudelft.nl; K.N.vanDalen@tudelft.nl; J.M.DeOliveiraBarbosa@tudelft.nl; A.Metrikine@tudelft.nl

**Abstract:** This paper addresses the dynamic response of an infinitely long cylindrical structure embedded in an elastic half-space. The structure has a circular cross-section and its axis is parallel to the half-space surface. Excitation can be incident body waves or forces applied on the surface of the half-space and/or the structure. The model can be used to assess the integrity of structures when acted upon by seismic waves, to predict ground-borne vibration due to circulation of vehicles, and to infer about the safety of vehicles during earthquake events. Because the half-space and the structure surfaces possess different symmetries, the solution is not straightforward. In order to circumvent this difficulty, the physical domain is conformally mapped onto an auxiliary domain with a cylindrical symmetry, in which the free surface of the half-space and the surface of the structure are located at concentric cylindrical surfaces. The solution of the original boundary value problem is finally obtained by solving a set of algebraic equations. Truncation of the summation over circumferential modes is needed in the numerical implementation. Convergence tests, validations and comparisons of stresses and motions for two- and three-dimensional cases are presented and discussed as well as the advantages and disadvantages of the proposed method. Additionally, the effect of the presence of the tunnel is analysed by considering a limiting case of the half-space with just a cylindrical cavity of the same radius as the outer radius of the tunnel.

**Keywords:** Three-dimensional wave propagation; dynamic soil-structure interaction; underground structure; conformal mapping; steady-state dynamic response; semi-analytical solution

## 1. Introduction

The study of wave propagation in elastic solids has been of interest in seismology and civil engineering for a long time. Given the fact that more underground facilities (for instance, lifelines and tunnels) need to be designed and constructed with the development of the modern world, it is important to investigate the dynamic response of underground structures to either earthquake excitation or other dynamic loads if applicable. A detailed review of the earthquake response and seismic-resistant design of underground pipeline systems was presented by Ariman and Muleski [1]. The existing methods to solve the wave scattering problem by

different types of inclusions embedded in a full space or a half-space were reviewed by Stamos and Beskos [2]. The advantages and disadvantages of each method were discussed in detail.

The studies on three-dimensional wave scattering by inclusions are much less numerous than those on the two-dimensional ones. In this paper, a solution to the problem of the three-dimensional wave scattering by an infinitely long underground structure with a circular cross-section embedded in an elastic half-space is presented.

Special attention is paid to a comparison of the obtained results with those of the previous works dealing with the same type of underground structures as in this paper. Luco and de Barros [3] investigated the two-dimensional response of a viscoelastic half-space containing a buried infinitely long cylindrical cavity of circular cross-section subjected to harmonic plane SH, P, SV and Rayleigh waves by using an indirect boundary integral method based on two-dimensional Green's functions for a viscoelastic half-space. They also obtained the three-dimensional response of an infinitely long cylindrical shell of circular cross-section embedded in a layered viscoelastic half-space and subjected to harmonic waves impinging at an oblique angle with respect to the longitudinal axis of the shell [4, 5]. The procedure employed in the latter references combines an indirect integral representation for the field in the exterior half-space with a model of the pipeline or tunnel based on the Donnell shell theory. The integral representation for the soil is based on the use of the so-called moving Green's functions for the layered viscoelastic half-space. In the paper [5], the authors validated the accuracy of the proposed method by extensive comparisons with the work by Wong et al. [6] who used the cylindrical eigenfunctions method and the work by Liu et al. [7] who used the boundary integral representation and finite element method for the three-dimensional cases. They also compared their results with those presented by Datta et al. [8] who employed a hybrid technique combining a finite element method with the eigenfunction expansion, Balendra et al. [9] who applied the method of wave function expansion and the image technique, Wong [6], and Liu [7] for the two-dimensional cases.

In this paper, a semi-analytical method is proposed to calculate the scattering of elastic waves by an infinitely long cylindrical structure of circular cross-section embedded in an linearly elastic, isotropic and homogeneous half-space. The method can be considered to be a straightforward extension of the method used to solve the two-dimensional scattering problems of P, SV, Rayleigh waves [10] and SH waves [11].

When the scattered waves from the underground structure (tunnel) impinge on the half-space surface, a secondary reflected wave field is generated (the primary reflected wave field is generated directly by the incident plane wave that excites the system). In the spirit of the image technique [12], the latter are sought for in the form of cylindrical waves that are generated by an imaginary source of an *apriori* unknown intensity placed at the image point that is positioned symmetrically to the centre of the tunnel with respect to the half-space surface. One of the aims of this paper is to evaluate the contributions of the wave field directly scattered by the tunnel and the secondary reflected wave filed on the dynamic response of the

system at the half-space surface and at the half-space interface with the tunnel. Different circumferential modes are taken into account in this evaluation and various convergence tests are presented. The hoop stresses and motions at the interface with the tunnel as well as the ground surface motions are also analysed for two- and three-dimensional cases in order to investigate the effects of the dimension and the presence of the tunnel on the system response.

## 2. Statement of the problem

Fig. 1 defines the problem to be analysed: an infinitely long cylindrical tunnel with a circular cross-section, whose axis is parallel to the half-space surface, is subjected to plane harmonic body waves of arbitrary propagation direction, which results in a three-dimensional problem. The materials of both the half-space and the tunnel are assumed isotropic and linearly elastic, and characterized by the Lamé parameters $\lambda_i$, $\mu_i$ and densities $\rho_i$ (the subscripts $i = 1, 2$ refer to the half-space and the tunnel, respectively). The centre of the tunnel ( $o_1$ ) is at depth $h$ beneath the half-space surface. $o_2$ is the image point that is positioned symmetrically to the centre of the tunnel with respect to the half-space surface. $R_I$, $R_O$ and $R_C$ stand for the inner and outer radii of the tunnel, and the centre line of the tunnel, respectively. To aid in the mathematical description of the different waves, six reference systems are represented: the global Cartesian ( $xyz$ ) and cylindrical ( $xr\Theta$ ) coordinate systems, the local Cartesian ( $xy_1z_1$ ) and cylindrical ( $xr_1\Theta_1$ ) coordinate systems centred at the tunnel, and ( $xy_2z_2$ ) and ( $xr_2\Theta_2$ ) originated at the image of the tunnel. Anti-clockwise is defined as the positive direction in the cylindrical coordinate systems.

The time dependence of the incident plane harmonic wave and the response of the system to this wave are assumed to be harmonic and proportional to $e^{-i\omega t}$, where $i = \sqrt{-1}$ is the imaginary unit and $\omega$ is the angular frequency of the wave. In what follows, the factor $e^{-i\omega t}$ will be dropped from all the expressions for brevity. The angle between the incident wave direction and the vertical axis $z$ is $\theta_v$ (see Fig. 1 (b), $\theta_v = 0$ for vertical incidence). The horizontal projection of the propagation direction on $xoy$ plane forms an angle $\theta_h$ (see Fig. 1 (c)) with the $x$ axis. The regions $\Omega_1$ and $\Omega_2$ refer to the domains of the soil medium and the tunnel, respectively.

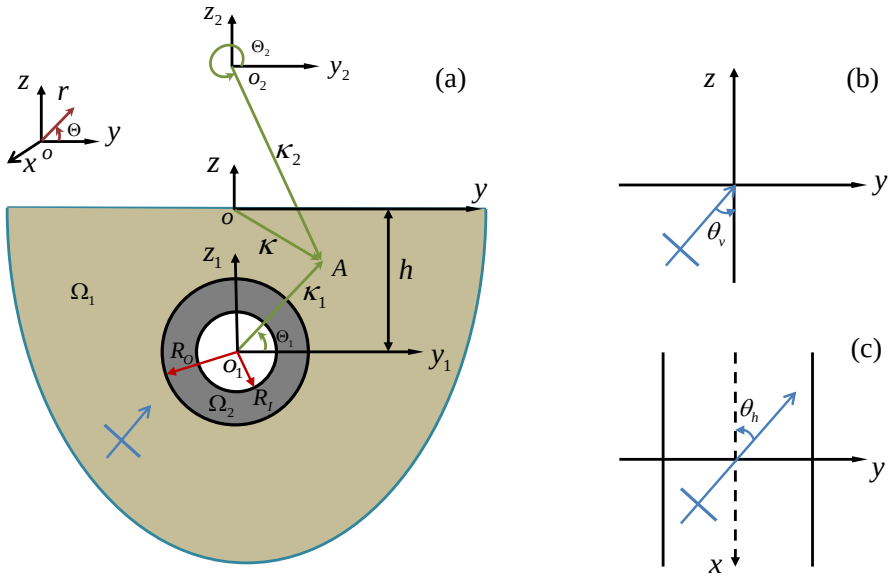


**Fig. 1** (a) The cross-section of the model; (b) The vertical incident angle; (c) The horizontal incident angle

### *2.1. Governing equations*

In the absence of the body forces, the equations of motion in the mediums in terms of the displacement vectors $\mathbf{u}_i$ can be written as

$$\left(\lambda_i+\mu_i\right)\nabla\nabla\cdot\mathbf{u}_i+\mu_i\nabla^2\mathbf{u}_i=\rho_i\ddot{\mathbf{u}}_i \tag{1}$$

Substituting the Helmholtz decomposition $\mathbf{u}_i=\nabla\phi_i+\nabla\times\boldsymbol{\psi}_i$ into the governing equation Eq (1), we obtain two uncoupled scalar and vector potential Helmholtz equations:

$$\nabla^2\phi_i+k_{pi}^2\phi_i=0 \tag{2}$$

$$\nabla^2\boldsymbol{\Psi}_i+k_{si}^2\boldsymbol{\Psi}_i=0 \tag{3}$$

where $\phi_i$ and $\boldsymbol{\Psi}_i$ are the compressional and shear wave potentials, respectively, $k_{pi}=\omega/c_{pi}$ and $k_{si}=\omega/c_{si}$ are the compressional and shear wavenumbers, respectively, and $c_{pi}=\sqrt{\left(\lambda_i+2\mu_i\right)/\rho_i}$ and $c_{si}=\sqrt{\mu_i/\rho_i}$ are the velocities of the compressional and shear waves, respectively.

The vector wave potential $\boldsymbol{\Psi}_i$ is chosen to satisfy the gauge condition

$\nabla \cdot \Psi_i = 0$, therefore, only two of the three components of $\Psi_i$ are independent. Correspondingly, Eq. (3) can be reduced to two uncoupled scalar Helmholtz equations [13, 14]

$$\nabla^2 \psi_i + k_{si}^2 \psi_i = 0 \tag{4}$$

$$\nabla^2 \chi_i + k_{si}^2 \chi_i = 0 \tag{5}$$

by defining the vector wave potentials $\Psi_i$ as

$$\Psi_{ii} = \Psi_{i1} + \Psi_{i2} \tag{6}$$

$$\Psi_{i1} = \psi_i e_x + \frac{1}{k_{si}^2} \nabla \left( \frac{\partial \psi_i}{\partial x} \right) \tag{7}$$

$$\Psi_{i2} = \frac{1}{k_{si}} \nabla \times (\chi_i e_x) \tag{8}$$

in which $e_x$ is the unit vector along $x$ axis.

The displacement fields are written in terms of the scalar wave potentials $\phi_i$, $\psi_i$ and $\chi_i$ as

$$u_{xi} = \frac{\partial \phi_i}{\partial x} + \frac{1}{k_{si}} \left( k_{si}^2 \chi_i + \frac{\partial^2 \chi_i}{\partial x^2} \right) \tag{9}$$

$$u_{yi} = \frac{\partial \phi_i}{\partial y} + \frac{\partial \psi_i}{\partial z} + \frac{1}{k_{si}} \frac{\partial^2 \chi_i}{\partial x \partial y} \tag{10}$$

$$u_{zi} = \frac{\partial \phi_i}{\partial z} - \frac{\partial \psi_i}{\partial y} + \frac{1}{k_{si}} \frac{\partial^2 \chi_i}{\partial x \partial z} \tag{11}$$

The stress components can be derived by the Hooke's law [15]. The displacement vector $\mathbf{u}$ and stress tensor $\boldsymbol{\sigma}$, where the subscript $i$ is omitted for brevity, can be further written in the cylindrical coordinate system defined as $y = r\cos\Theta$ and $z = r\sin\Theta$ according to the linear transformation

$$\begin{bmatrix} u_x \\ u_r \\ u_\theta \end{bmatrix} = \begin{bmatrix} 1 & 0 & 0 \\ 0 & \cos\Theta & \sin\Theta \\ 0 & -\sin\Theta & \cos\Theta \end{bmatrix} \begin{bmatrix} u_x \\ u_y \\ u_z \end{bmatrix} \tag{12}$$

$$\begin{bmatrix} \sigma_{xx} & \sigma_{xr} & \sigma_{x\theta} \\ \sigma_{rx} & \sigma_{rr} & \sigma_{r\theta} \\ \sigma_{\theta x} & \sigma_{\theta r} & \sigma_{\theta\theta} \end{bmatrix} = \begin{bmatrix} 1 & 0 & 0 \\ 0 & \cos\Theta & \sin\Theta \\ 0 & -\sin\Theta & \cos\Theta \end{bmatrix} \begin{bmatrix} \sigma_{xx} & \sigma_{xy} & \sigma_{xz} \\ \sigma_{yx} & \sigma_{yy} & \sigma_{yz} \\ \sigma_{zx} & \sigma_{zy} & \sigma_{zz} \end{bmatrix} \begin{bmatrix} 1 & 0 & 0 \\ 0 & \cos\Theta & -\sin\Theta \\ 0 & \sin\Theta & \cos\Theta \end{bmatrix} \tag{13}$$

This transformation is instrumental for description of the cylindrical displacements and stresses at the tunnel surfaces.

### *2.2. Boundary conditions*

The method presented in this paper is general. It can be applied to analyse the dynamic response of the tunnel embedded in a half-space to either external dynamic forces or seismic waves. Considering the problem of vehicles moving either along the half-space surface or through the tunnel, external traction vector are acting either on the half-space surface ( $\boldsymbol{\sigma}^{ext1} = [\sigma_{zz}, \sigma_{zy}, \sigma_{zx}]$ ) or on the inner surface of the tunnel ( $\boldsymbol{\sigma}^{ext2} = [\sigma_{rr}, \sigma_{r\theta}, \sigma_{rx}]$ ). The boundary conditions considering, for generality, both of the above excitations are written as

$$[\sigma_{zz1}, \sigma_{zy1}, \sigma_{zx1}] = \boldsymbol{\sigma}^{ext1}, \qquad z = 0 \qquad (14)$$

$$[\sigma_{rr2}, \sigma_{r\theta 2}, \sigma_{rx2}] = \boldsymbol{\sigma}^{ext2}, \qquad r_1 = R_I \qquad (15)$$

If only the incident harmonic plane wave excites the system, the external stresses acting on the half-space surface and the inner surface of the tunnel will vanish, resulting in the traction-free boundary conditions at these surfaces.

We assume that the contact condition between the soil medium and the tunnel is perfect. This implies that there is neither partial nor full slip motion at the soil-tunnel interface and there is also no separation at the soil-tunnel interface along normal direction, which results in continuity conditions of all tractions and displacements. The equilibrium of the tractions and compatibility of the displacements at the soil-tunnel interface can be written as

$$\sigma_{rr1} = \sigma_{rr2},\ \sigma_{r\theta 1} = \sigma_{r\theta 2},\ \sigma_{rx1} = \sigma_{rx2}, \qquad r_1 = R_O \qquad (16)$$

$$u_{r1} = u_{r2},\ u_{\theta 1} = u_{\theta 2},\ u_{x1} = u_{x2}, \qquad r_1 = R_O \qquad (17)$$

To demonstrate the merit of the proposed method, in what follows, we consider a harmonic compressional wave as external excitation.

## 3. Solutions of the governing equations

In this section, the obtained solutions of the governing equations using the method of separation of variables are given in the Cartesian and cylindrical coordinate systems [13]. These solutions are used to construct the complete wave field in the system [15].

### *3.1. The incident and the primary reflected waves*

In the absence of the underground structure in the half-space, the wave field is the sum of the incident ( $\phi^i$ ) and the primary reflected wave fields ( $\phi^r$ , $\psi^r$ , $\chi^r$ ):

$$\phi^i = \phi_0 e^{\mathrm{i}k_x x + \mathrm{i}k_y y + \mathrm{i}k_{pz1} z} \tag{18}$$

$$\phi^r = A\phi_0 e^{\mathrm{i}k_x x + \mathrm{i}k_y y - \mathrm{i}k_{pz1} z} \tag{19}$$

$$\psi^r = B\phi_0 e^{\mathrm{i}k_x x + \mathrm{i}k_y y - \mathrm{i}k_{sz1} z} \tag{20}$$

$$\chi^r = C\phi_0 e^{\mathrm{i}k_x x + \mathrm{i}k_y y - \mathrm{i}k_{sz1} z} \tag{21}$$

with $\phi_0$ the amplitude of the incident compressional wave, $A$, $B$ and $C$ the unknown coefficients of the primary reflected waves $\phi^r$ , $\psi^r$ and $\chi^r$ , respectively, $k_x = -\omega / c_{p1} \sin(\theta_v)\cos(\theta_h)$ and $k_y = \omega / c_{p1} \sin(\theta_v)\sin(\theta_h)$ the wave numbers along $x$ and $y$ axis, respectively, $c_{p1}$ the velocity of the incident wave, $k_{pz1} = \sqrt{k_{p1}^2 - k^2}$ and $k_{sz1} = \sqrt{k_{s1}^2 - k^2}$ the wave numbers of the compressional and shear waves along $z$ axis in the soil medium, respectively, $k^2 = {k_x}^2 + {k_y}^2$ . The unknown coefficients $A$, $B$ and $C$ can be determined by satisfying the traction free boundary conditions at the half-space surface.

### *3.2. Wave fields generated due to the presence of the tunnel*

Due to the presence of the tunnel, the scattered compressional and shear waves are generated at the outer surface of the tunnel; they are denoted as $\phi_{11}^s$ , $\psi_{11}^s$ , $\chi_{11}^s$ , respectively. When these scattered waves impinge on the half-space surface, a secondary reflected wave field is generated. In the spirit of the image technique [12], the generated secondary reflected waves are sought for in the form of cylindrical waves that are generated by an imaginary source of an *apriori* unknown intensity placed at $o_2$ (see Fig. 1), and denoted as $\phi_{12}^s$ , $\psi_{12}^s$ , $\chi_{12}^s$ . All these wave potentials satisfy the Helmholtz equations in the two cylindrical coordinate systems shown in Fig. 1 (the origins of these systems are located at $o_1$ and $o_2$ ) and are expressed as [13]

$$\phi_{11}^s = \sum_{n=-\infty}^{\infty} a_n H_n^{(1)}(k_{\alpha 1} r_1) e^{\mathrm{i}n\Theta_1} e^{\mathrm{i}k_x x} \tag{22}$$

$$\psi_{11}^s = \sum_{n=-\infty}^{\infty} b_n H_n^{(1)}(k_{\beta 1} r_1) e^{\mathrm{i}n\Theta_1} e^{\mathrm{i}k_x x} \tag{23}$$

$$\chi_{11}^{s}=\sum_{n=-\infty}^{\infty}c_{n}H_{n}^{(1)}(k_{\beta1}r_{1})e^{in\Theta_{1}}e^{ik_{x}x} \tag{24}$$

$$\phi_{12}^{s}=\sum_{n=-\infty}^{\infty}d_{n}H_{n}^{(1)}(k_{\alpha1}r_{2})e^{in\Theta_{2}}e^{ik_{x}x} \tag{25}$$

$$\psi_{12}^{s}=\sum_{n=-\infty}^{\infty}e_{n}H_{n}^{(1)}(k_{\beta1}r_{2})e^{in\Theta_{2}}e^{ik_{x}x} \tag{26}$$

$$\chi_{12}^{s}=\sum_{n=-\infty}^{\infty}f_{n}H_{n}^{(1)}(k_{\beta1}r_{2})e^{in\Theta_{2}}e^{ik_{x}x} \tag{27}$$

where $H_n^{(1)}$ denotes the Hankel function of the first kind and order $n$, and stands for outgoing (propagating from the tunnel) waves considering the time dependent factor $e^{-i\omega t}$. $k_{a1}=\sqrt{k_{p1}^2-k_x^2}$ and $k_{\beta1}=\sqrt{k_{s1}^2-k_x^2}$ are the cylindrical wave numbers of the compressional and shear waves in the soil medium, respectively.

The wave fields in the tunnel also satisfy the Helmholtz equations in the cylindrical coordinate system and are written as

$$\phi_{2}^{s}=\sum_{n=-\infty}^{\infty}g_{n}H_{n}^{(1)}(k_{\alpha2}r_{1})e^{in\Theta_{1}}e^{ik_{x}x}+\sum_{n=-\infty}^{\infty}h_{n}H_{n}^{(2)}(k_{\alpha2}r_{1})e^{in\Theta_{1}}e^{ik_{x}x} \tag{28}$$

$$\psi_{2}^{s}=\sum_{n=-\infty}^{\infty}i_{n}H_{n}^{(1)}(k_{\beta2}r_{1})e^{in\Theta_{1}}e^{ik_{x}x}+\sum_{n=-\infty}^{\infty}j_{n}H_{n}^{(2)}(k_{\beta2}r_{1})e^{in\Theta_{1}}e^{ik_{x}x} \tag{29}$$

$$\chi_{2}^{s}=\sum_{n=-\infty}^{\infty}k_{n}H_{n}^{(1)}(k_{\beta2}r_{1})e^{in\Theta_{1}}e^{ik_{x}x}+\sum_{n=-\infty}^{\infty}l_{n}H_{n}^{(2)}(k_{\beta2}r_{1})e^{in\Theta_{1}}e^{ik_{x}x} \tag{30}$$

where $H_n^{(2)}$ denotes the Hankel function of the second kind and order $n$, and stands for ingoing (propagating towards the origin of the coordinate system) waves considering the time dependent factor $e^{-i\omega t}$. $k_{a2}=\sqrt{k_{p2}^2-k_x^2}$ and $k_{\beta2}=\sqrt{k_{s2}^2-k_x^2}$ are the cylindrical wave numbers of the compressional and shear waves in the tunnel, respectively. According to the phase matching principle, in both the soil medium and the tunnel, the wavenumbers of the compressional and shear waves along $x$ axis are the same as in the incident wave and, accordingly, are equal to $k_x$. The unknown coefficients in Eqs. (22)-(30) will be determined from the boundary conditions.

### *3.3. Total wave fileds*

The total wave field in the soil medium ($\phi_1$, $\psi_1$ and $\chi_1$) consist of the incident, primary reflected, scattered and secondary reflected wave fields. The total wave field in the tunnel ($\phi_2$, $\psi_2$ and $\chi_2$) are the sum of outgoing and ingoing wave

fields.

$$\phi_1 = \phi^i + \phi^r + +\phi_{11}^s + \phi_{12}^s \tag{31}$$

$$\psi_1 = \psi^r + \psi_{11}^s + \psi_{12}^s \tag{32}$$

$$\chi_1 = \chi^r + \chi_{11}^s + \chi_{12}^s \tag{33}$$

$$\phi_2 = \phi_2^s \tag{34}$$

$$\psi_2 = \psi_2^s \tag{35}$$

$$\chi_2 = \chi_2^s \tag{36}$$

## 4. Stresses and displacements expressed in terms of complex variables

In this section, we introduce a complex variable $\kappa = y + \mathrm{i}z = re^{\mathrm{i}\Theta}$ and its conjugate $\bar{\kappa} = y - \mathrm{i}z = re^{-\mathrm{i}\Theta}$, where $y$, $z$ and $r$, $\Theta$ are the Cartesian and cylindrical coordinates introduced earlier. Using those, the polar angles $\Theta_1$ and $\Theta_2$ related to the local coordinate systems in Fig. 1 (a) can be written in terms of the complex variable $\kappa$ related to the global coordinate system as

$$e^{\mathrm{i}\Theta_1} = \frac{\kappa_1}{|\kappa_1|} = \frac{\kappa + \mathrm{i}h}{|\kappa + \mathrm{i}h|} \tag{37}$$

$$e^{\mathrm{i}\Theta_2} = \frac{\kappa_2}{|\kappa_2|} = \frac{\kappa - \mathrm{i}h}{|\kappa - \mathrm{i}h|} \tag{38}$$

The components of the displacements and stresses in Cartesian coordinates $xyz$ can be expressed in terms of the complex variables $\kappa$ and $\bar{\kappa}$ as

$$u_{xi} = \mathrm{i}k_x\phi_i + \frac{k_{\beta i}^2}{k_{si}}\chi_i \tag{39}$$

$$u_{yi} = \left(\frac{\partial\phi_i}{\partial\kappa} + \frac{\partial\phi_i}{\partial\bar{\kappa}}\right) + \mathrm{i}\left(\frac{\partial\psi_i}{\partial\kappa} - \frac{\partial\psi_i}{\partial\bar{\kappa}}\right) + \frac{\mathrm{i}k_x}{k_{si}}\left(\frac{\partial\chi_i}{\partial\kappa} + \frac{\partial\chi_i}{\partial\bar{\kappa}}\right) \tag{40}$$

$$u_{zi} = \mathrm{i}\left(\frac{\partial\phi_i}{\partial\kappa} - \frac{\partial\phi_i}{\partial\bar{\kappa}}\right) - \left(\frac{\partial\psi_i}{\partial\kappa} + \frac{\partial\psi_i}{\partial\bar{\kappa}}\right) + \frac{-k_x}{k_{si}}\left(\frac{\partial\chi_i}{\partial\kappa} - \frac{\partial\chi_i}{\partial\bar{\kappa}}\right) \tag{41}$$

$$\sigma_{xxi} = -(\lambda_i + 2\mu_i)k_x^2\phi_i - \lambda_i k_{\alpha i}^2\phi_i + \frac{2\mathrm{i}\mu_i k_x k_{\beta i}^2}{k_{si}}\chi_i \tag{42}$$

$$\sigma_{yyi} = -\lambda_i k_x^2 \phi_i - \left(\lambda_i + \mu_i\right) k_{\alpha i}^2 \phi_i + 2\mu_i \left( \frac{\partial^2 \phi_i}{\partial \kappa^2} + \frac{\partial^2 \phi_i}{\partial \bar{\kappa}^2} \right) + 2\mathrm{i}\mu_i \left( \frac{\partial^2 \psi_i}{\partial \kappa^2} - \frac{\partial^2 \psi_i}{\partial \bar{\kappa}^2} \right)$$
$$- \frac{\mathrm{i}\mu_i k_x k_{\beta i}^2}{k_{si}} \chi_i + \frac{2\mathrm{i}\mu_i k_x}{k_{si}} \left( \frac{\partial^2 \chi_i}{\partial \kappa^2} + \frac{\partial^2 \chi_i}{\partial \bar{\kappa}^2} \right) \tag{43}$$

$$\sigma_{yxi} = 2\mathrm{i}\mu_i k_x \left( \frac{\partial \phi_i}{\partial \kappa} + \frac{\partial \phi_i}{\partial \bar{\kappa}} \right) - \mu_i k_x \left( \frac{\partial \psi_i}{\partial \kappa} - \frac{\partial \psi_i}{\partial \bar{\kappa}} \right)$$
$$+ \frac{\mu_i \left( k_{si}^2 - 2k_x^2 \right)}{k_{si}} \left( \frac{\partial \chi_i}{\partial \kappa} + \frac{\partial \chi_i}{\partial \bar{\kappa}} \right) \tag{44}$$

$$\sigma_{zzi} = -\lambda_i k_x^2 \phi_i - \left(\lambda_i + \mu_i\right) k_{\alpha i}^2 \phi_i - 2\mu_i \left( \frac{\partial^2 \phi_i}{\partial \kappa^2} + \frac{\partial^2 \phi_i}{\partial \bar{\kappa}^2} \right) - 2\mathrm{i}\mu_i \left( \frac{\partial^2 \psi_i}{\partial \kappa^2} - \frac{\partial^2 \psi_i}{\partial \bar{\kappa}^2} \right)$$
$$- \frac{\mathrm{i}\mu_i k_x k_{\beta i}^2}{k_{si}} \chi_i - \frac{2\mathrm{i}\mu_i k_x}{k_{si}} \left( \frac{\partial^2 \chi_i}{\partial \kappa^2} + \frac{\partial^2 \chi_i}{\partial \bar{\kappa}^2} \right) \tag{45}$$

$$\sigma_{zyi} = 2\mathrm{i}\mu_i \left( \frac{\partial^2 \phi_i}{\partial \kappa^2} - \frac{\partial^2 \phi_i}{\partial \bar{\kappa}^2} \right) - 2\mu_i \left( \frac{\partial^2 \psi_i}{\partial \kappa^2} + \frac{\partial^2 \psi_i}{\partial \bar{\kappa}^2} \right) - \frac{2\mu_i k_x}{k_{si}} \left( \frac{\partial^2 \chi_i}{\partial \kappa^2} - \frac{\partial^2 \chi_i}{\partial \bar{\kappa}^2} \right) \tag{46}$$

$$\sigma_{zxi} = -2\mu_i k_x \left( \frac{\partial \phi_i}{\partial \kappa} - \frac{\partial \phi_i}{\partial \bar{\kappa}} \right) - \mathrm{i}\mu_i k_x \left( \frac{\partial \psi_i}{\partial \kappa} + \frac{\partial \psi_i}{\partial \bar{\kappa}} \right)$$
$$+ \frac{\mathrm{i}\mu_i \left( k_{si}^2 - 2k_x^2 \right)}{k_{si}} \left( \frac{\partial \chi_i}{\partial \kappa} - \frac{\partial \chi_i}{\partial \bar{\kappa}} \right) \tag{47}$$

By applying the transformation relations between the Cartesian and cylindrical coordinate systems (Eqs. (12)-(13)), the expressions for the displacements and stresses in the cylindrical coordinate system $xr\Theta$ can be written in terms of the variables $\kappa$ and $\bar{\kappa}$ as

$$u_{ri} = \left( e^{\mathrm{i}\Theta} \frac{\partial \phi_i}{\partial \kappa} + e^{-\mathrm{i}\Theta} \frac{\partial \phi_i}{\partial \bar{\kappa}} \right) + \mathrm{i} \left( e^{\mathrm{i}\Theta} \frac{\partial \psi_i}{\partial \kappa} - e^{-\mathrm{i}\Theta} \frac{\partial \psi_i}{\partial \bar{\kappa}} \right)$$
$$+ \frac{\mathrm{i}k_x}{k_{si}} \left( e^{\mathrm{i}\Theta} \frac{\partial \chi_i}{\partial \kappa} + e^{-\mathrm{i}\Theta} \frac{\partial \chi_i}{\partial \bar{\kappa}} \right) \tag{48}$$

$$u_{\theta i} = \mathrm{i} \left( e^{\mathrm{i}\Theta} \frac{\partial \phi_i}{\partial \kappa} - e^{-\mathrm{i}\Theta} \frac{\partial \phi_i}{\partial \bar{\kappa}} \right) - \left( e^{\mathrm{i}\Theta} \frac{\partial \psi_i}{\partial \kappa} + e^{-\mathrm{i}\Theta} \frac{\partial \psi_i}{\partial \bar{\kappa}} \right)$$
$$+ \frac{-k_x}{k_{si}} \left( e^{\mathrm{i}\Theta} \frac{\partial \chi_i}{\partial \kappa} - e^{-\mathrm{i}\Theta} \frac{\partial \chi_i}{\partial \bar{\kappa}} \right) \tag{49}$$

$$u_{xi} = \mathrm{i}k_x \phi_i + \frac{k_{\beta i}^2}{k_{si}} \chi_i \tag{50}$$

$$\sigma_{rri} = -\lambda_i k_x^2 \phi_i - (\lambda_i + \mu_i) k_{\alpha i}^2 \phi_i + 2\mu_i \left( e^{2i\Theta} \frac{\partial^2 \phi_i}{\partial \kappa^2} + e^{-2i\Theta} \frac{\partial^2 \phi_i}{\partial \bar{\kappa}^2} \right) - \frac{i\mu_i k_x k_{\beta i}^2}{k_{si}} \chi_i$$
$$+2i\mu_i \left( e^{2i\Theta} \frac{\partial^2 \psi_i}{\partial \kappa^2} - e^{-2i\Theta} \frac{\partial^2 \psi_i}{\partial \bar{\kappa}^2} \right) + \frac{2i\mu_i k_x}{k_{si}} \left( e^{2i\Theta} \frac{\partial^2 \chi_i}{\partial \kappa^2} + e^{-2i\Theta} \frac{\partial^2 \chi_i}{\partial \bar{\kappa}^2} \right) \tag{51}$$

$$\sigma_{r\theta i} = 2i\mu_i \left( e^{2i\Theta} \frac{\partial^2 \phi_i}{\partial \kappa^2} - e^{-2i\Theta} \frac{\partial^2 \phi_i}{\partial \bar{\kappa}^2} \right) - 2\mu_i \left( e^{2i\Theta} \frac{\partial^2 \psi_i}{\partial \kappa^2} + e^{-2i\Theta} \frac{\partial^2 \psi_i}{\partial \bar{\kappa}^2} \right)$$
$$- \frac{2\mu_i k_x}{k_{si}} \left( e^{2i\Theta} \frac{\partial^2 \chi_i}{\partial \kappa^2} - e^{-2i\Theta} \frac{\partial^2 \chi_i}{\partial \bar{\kappa}^2} \right) \tag{52}$$

$$\sigma_{rxi} = 2i\mu_i k_x \left( e^{i\Theta} \frac{\partial \phi_i}{\partial \kappa} + e^{-i\Theta} \frac{\partial \phi_i}{\partial \bar{\kappa}} \right) - \mu_i k_x \left( e^{i\Theta} \frac{\partial \psi_i}{\partial \kappa} - e^{-i\Theta} \frac{\partial \psi_i}{\partial \bar{\kappa}} \right)$$
$$+ \frac{\mu_i \left( k_{si}^2 - 2k_x^2 \right)}{k_{si}} \left( e^{i\Theta} \frac{\partial \chi_i}{\partial \kappa} + e^{-i\Theta} \frac{\partial \chi_i}{\partial \bar{\kappa}} \right) \tag{53}$$

$$\sigma_{\theta\theta i} = -\lambda_i k_x^2 \phi_i - (\lambda_i + \mu_i) k_{\alpha i}^2 \phi_i - 2\mu_i \left( e^{2i\Theta} \frac{\partial^2 \phi_i}{\partial \kappa^2} + e^{-2i\Theta} \frac{\partial^2 \phi_i}{\partial \bar{\kappa}^2} \right) - \frac{i\mu_i k_x k_{\beta i}^2}{k_{si}} \chi_i$$
$$-2i\mu_i \left( e^{2i\Theta} \frac{\partial^2 \psi_i}{\partial \kappa^2} - e^{-2i\Theta} \frac{\partial^2 \psi_i}{\partial \bar{\kappa}^2} \right) - \frac{2i\mu_i k_x}{k_{si}} \left( e^{2i\Theta} \frac{\partial^2 \chi_i}{\partial \kappa^2} + e^{-2i\Theta} \frac{\partial^2 \chi_i}{\partial \bar{\kappa}^2} \right) \tag{54}$$

$$\sigma_{\theta x i} = -2\mu_i k_x \left( e^{i\Theta} \frac{\partial \phi_i}{\partial \kappa} - e^{-i\Theta} \frac{\partial \phi_i}{\partial \bar{\kappa}} \right) - i\mu_i k_x \left( e^{i\Theta} \frac{\partial \psi_i}{\partial \kappa} + e^{-i\Theta} \frac{\partial \psi_i}{\partial \bar{\kappa}} \right)$$
$$+ \frac{i\mu_i \left( k_{si}^2 - 2k_x^2 \right)}{k_{si}} \left( e^{i\Theta} \frac{\partial \chi_i}{\partial \kappa} - e^{-i\Theta} \frac{\partial \chi_i}{\partial \bar{\kappa}} \right) \tag{55}$$

## 5. Conformal mapping

The problem under consideration is complicated by the fact that the half-space and the tunnel surfaces possess different symmetries. In order to circumvent this difficulty, the physical domain is mapped onto an auxiliary domain represented by a complex variable $\zeta = \xi + i\eta = \rho e^{i\theta}$ and its conjugate $\bar{\zeta} = \xi - i\eta = \rho e^{-i\theta}$. We search for two mapping functions to map the two regions $\Omega_1$ and $\Omega_2$ in the physical domain (as shown in Fig. 1) onto regions $\Gamma_1$ and $\Gamma_2$ in the image domain (as shown in Fig. 2), respectively, and make the two regions in the image domain possess the same symmetry and be concentric.

The transformation of the region $\Omega_1$ in the physical domain into the region $\Gamma_1$ in the image domain is accomplished by the mapping function [16]

$$\kappa_1 = w_1(\zeta) = -\mathrm{i}T\frac{1+\zeta}{1-\zeta} \tag{56}$$

Where $T = h\left(1-\alpha_O^2\right)/\left(1+\alpha_O^2\right)$, $\alpha_O = h/R_O - \sqrt{\left(h/R_O\right)^2 - 1}$. The half-space surface and the outer surface of the tunnel in the physical domain correspond to the circles $|\zeta| = 1$ and $|\zeta| = \alpha_O$ in the image domain, respectively.

The second mapping function determines a transformation of the region $\Omega_2$ into the region $\Gamma_2$:

$$\kappa_2 = w_2(\zeta) = -\mathrm{i}h + \frac{R_O}{\alpha_O}\zeta \tag{57}$$

The outer and inner surfaces of the tunnel in the physical domain correspond to the circles $|\zeta| = \alpha_O$ and $|\zeta| = \alpha_I = R_I\alpha_O / R_O$ in the image domain, respectively.

The relation between the angle $\Theta$ in the physical domain and the polar angle $\theta$ in the image domain is written as [17]

$$\exp\left(\mathrm{i}\Theta\right) = \frac{\zeta}{\rho}\frac{w'(\zeta)}{|w'(\zeta)|} \tag{58}$$

It can be shown that the mapping functions $w_1(\zeta)$ and $w_2(\zeta)$ are analytic and their derivatives $w_1'(\zeta)$ and $w_2'(\zeta)$ are not zero in the regions $\Gamma_1$ and $\Gamma_2$, which ensures the transformation be conformal, reversible and single-valued in each domain.

Using conformal mapping functions $w_1(\zeta)$ and $w_2(\zeta)$, a point $B$ at the outer surface of the tunnel in the physical domain (see Fig. 1) is mapped to two different points $B^+$ and $B^-$ in the image domain (as shown in Fig. 2), respectively. When we apply the continuity conditions at the soil-tunnel interface, we have to consider this discontinuous relation at $|\zeta| = \alpha_O$ in the image domain. Let $\theta^+$ and $\theta$ denote the angles between the vectors $\overrightarrow{OB^+}$ and $\overrightarrow{OB^-}$, and the horizontal axis in the image plane, respectively. The relation between these two angles is given as

$$\theta^+(\theta) = \arg\left[\frac{\mathrm{i}R_O e^{\mathrm{i}\theta} + h - T}{\mathrm{i}R_O e^{\mathrm{i}\theta} + h + T}\right] \tag{59}$$

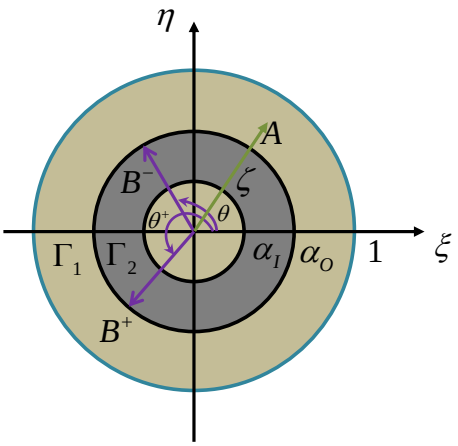


**Fig. 2** Image domain

## 6. Derivation of the unknown coefficients using boundary conditions

The traction-free boundary conditions at the half-space surface and at the inner surface of the tunnel, and the continuity conditions of the tractions and displacements at the soil-tunnel interface lead to a linear system of equations in terms of the unknown coefficients.

Based on the relation between the complex variables $\kappa$ and $\zeta$ defined by the conformal mapping functions (Eqs. (56)-(57)), the wave potentials and the expressions for the displacements and stresses can be derived in terms of the complex variables $\zeta$ and $\bar{\zeta}$. The expressions are not given in this paper for brevity, they are similar to those presented in the papers on the two-dimensional problems [10, 11]. The derivatives of the cylindrical wave potentials with respect to the complex variables are given by Liu et al in [18]. Substituting Eqs. (31)-(36) into Eqs. (45)-(53) and taking into account the formulated boundary conditions (14)-(17) we obtain a set of algebraic equations in terms of the complex variables $\kappa$ and $\bar{\kappa}$. Finally, using the mapping functions (Eqs. (56)-(57)), a set of algebraic equations in terms of the complex variables $\zeta$ and $\bar{\zeta}$ can be formulated as

$$\sum_{i=1}^{12}\sum_{n=-\infty}^{\infty} K_n^{(ij)} X_n^{(i)} = R^{(j)}, \ (j = 1,...,12) \tag{60}$$

where $X_n^{(1)} = a_n$ , $X_n^{(2)} = b_n$ , $X_n^{(3)} = c_n$ , $X_n^{(4)} = d_n$ , $X_n^{(5)} = e_n$ , $X_n^{(6)} = f_n$ , $X_n^{(7)} = g_n$, $X_n^{(8)} = h_n$, $X_n^{(9)} = i_n$, $X_n^{(10)} = j_n$, $X_n^{(11)} = k_n$, $X_n^{(12)} = l_n$; each $i$ and $j$ correspond to an unknown coefficient and a boundary condition, respectively.

$j=1,2,3$ refer to the traction-free boundary conditions at the half-space surface, $j=4,5,6$ refer to the traction-free boundary conditions at the inner surface of the tunnel, $j=7,8,9$ and $j=10,11,12$ refer to the traction and displacement continuity conditions at the soil-tunnel interface, respectively. $K_n^{(ij)}$ and $R^{(j)}$ are functions of the complex variables $\zeta$ and $\bar{\zeta}$; they are not given in this paper for brevity. For the set of algebraic equations ( $j=7-12$ ) formulated based on the continuity conditions, all the tractions and displacements related to soil medium, namely, $\sigma_{rr1}$, $\sigma_{r\theta 1}$, $\sigma_{rx1}$, $u_{r1}$, $u_{\theta 1}$ and $u_{x1}$, are functions of $\theta^+$ while those related to the tunnel are all functions of $\theta$.

It is obvious that $K_n^{(ij)}$ and $R^{(j)}$ are functions of $\theta$ in the image domain. Multiplying both sides of Eq. (60) by a weighting function $\exp(-\mathrm{i}s\theta)$ and integrating over the interval $[0,2\pi]$, we obtain:

$$\sum_{i=1}^{12}\sum_{n=-\infty}^{\infty} K_n^{(ijs)} X_n^{(i)} = R^{(js)},\ (j=1,...,12;\ s=0,\pm1,\pm2,...) \tag{61}$$

where $K_n^{(ijs)} = \int_0^{2\pi} K_n^{(ij)} \exp(-\mathrm{i}s\theta)\, d\theta/(2\pi)$ and $R_n^{(js)} = \int_0^{2\pi} R_n^{(j)} \exp(-\mathrm{i}s\theta)\, d\theta/(2\pi)$.

To compute the unknown coefficients, the summation over circumferential modes is truncated. When we use the same modes $N$ for both the waves scattered by the tunnel and the secondary reflected waves, we use the weighting function:

$$\exp(-\mathrm{i}s\theta),\ (j=1,...,12;\ s=0,\pm1,\pm2,...\pm N) \tag{62}$$

When we use $N$ modes for the directly scattered waves by the tunnel and $M$ modes for the secondary reflected waves, in order to formulate a square matrix, Eq (60) are multiplied by different weighting functions, according to

$$\begin{aligned} &\exp(-\mathrm{i}s_I\theta),\ (j=1,...,3;\ s_I=0,\pm1,\pm2,...,\pm M) \\ &\exp(-\mathrm{i}s\theta),\ (j=4,...,12;\ s=0,\pm1,\pm2,...,\pm N) \end{aligned} \tag{63}$$

## 7. Convergence tests, validations and numberical analysis

In this paper, a stiff soil medium and a concrete tunnel are considered. The stiff soil medium has a modulus of elasticity $E_1 = 7.567\cdot10^9\,\mathrm{N/m^2}$, Poisson's ratio $\upsilon_1 = 0.333$ and mass density $\rho_1 = 2.664\cdot10^3\,\mathrm{kg/m^3}$, while for the concrete tunnel

$E_2 = 1.6 \cdot 10^{10}\,\mathrm{N/m^2}$ , $\upsilon_2 = 0.2$ and $\rho_2 = 2.24 \cdot 10^3\,\mathrm{kg/m^3}$ . A dimensionless frequency is defined as $\varpi = \omega R_O / \pi c_{s1}$ . The normalized displacement vector and the stress tensor are given by $\mathbf{U} = \mathbf{u} / u_0$ and $\mathbf{\Sigma} = \boldsymbol{\sigma} / \left( \omega \rho_1 c_{s1} u_0 \right)$ , where $u_0$ denotes the displacement amplitude of the incident wave.

When the incident harmonic wave propagates in the direction perpendicular to the axis of the tunnel, the problem reduces to a two-dimensional one. Fig. 3 depicts various convergence tests for a two-dimensional wave scattering problem of a half-space with a cavity (limiting case of the half-space with just a cylindrical cavity of the same radius as the outer radius of the tunnel) under a relatively high excitation frequency of $\varpi = 0.5$ ( $f = 51$ Hz ). Figs. 3 (a-c) show that, considering $N = 6$ for the directly scattered waves by the cavity, 3 and 9 modes for the second reflected waves are needed to get the hoop stress ( $\Sigma_{\theta\theta}$ ) at the cavity surface and the ground surface motions ( $U_y$ , $U_z$ ) to converge, respectively. Figs. 3 (d-f) show that, considering $M = 9$ for the secondary reflected waves, 5 and 2 modes for the waves directly scattered by the cavity are needed to get the hoop stress and the ground surface motions to converge, respectively. Therefore, 5 modes for the directly scattered waves by the cavity and 9 modes for the secondary reflected waves are enough to represent the wave fields in the half-space due to presence of the cavity under the high-frequency excitation of $\varpi = 0.5$.

Fig. 4 depicts various convergence tests of a three-dimensional wave scattering problem of a tunnel embedded in the half-space under a low-frequency excitation of $\varpi = 0.105$ ( $f = 10.8$ Hz ). Figs. 4 (a-c) show that for the secondary reflected waves with $N = 3$, 3 modes are needed to get convergence for the hoop stress and the motion at the tunnel surface, as well as for the ground surface motion. Figs. 4 (d-f) show that for the waves directly scattered by the tunnel with $M = 3$, 3 modes are needed to get convergence for the hoop stress, while 2 modes are needed to get the convergence for the motions at both the tunnel and half-space surfaces. Therefore, 3 modes for both the directly scattered waves and the secondary reflected waves are sufficient to accurately represent the wave fields in the system under the low-frequency excitation of $\varpi = 0.105$.

As shown in Figs. 3 and 4, the results are in good agreement with those presented by Luco and de Barros [3] for the two-dimensional case and by de Barros and Luco [4, 5] for the three-dimensional case, which confirms the accuracy of the proposed method. There are some benefits of using different numbers of circumferential modes for the waves directly scattered by the tunnel and for the secondary reflected waves compared with the case of using the same number of modes for both waves as done in [10, 11]. The size and condition number of the coefficient matrix in Eq. (61) become smaller and the computational time is reduced. It is also helpful to understand that under low-frequency excitation only a few modes are needed to model the cylindrical waves fields due to presence of the tunnel, while under high-frequency excitation we need more modes to model the secondary reflected waves. In addition, the waves directly scattered by the tunnel affect the satisfaction of the boundary conditions and responses at the tunnel surfaces and barely affect those at the half-space surface. Correspondingly, the

secondary reflected waves contribute to the satisfaction of the boundary conditions and responses at the half-space surface and barely contribute to those at the tunnel surfaces. The reason for this phenomenon is the geometrical attenuation of the cylindrical waves. Obviously, the wave potentials have stronger contributions in the near field compared with the far field.

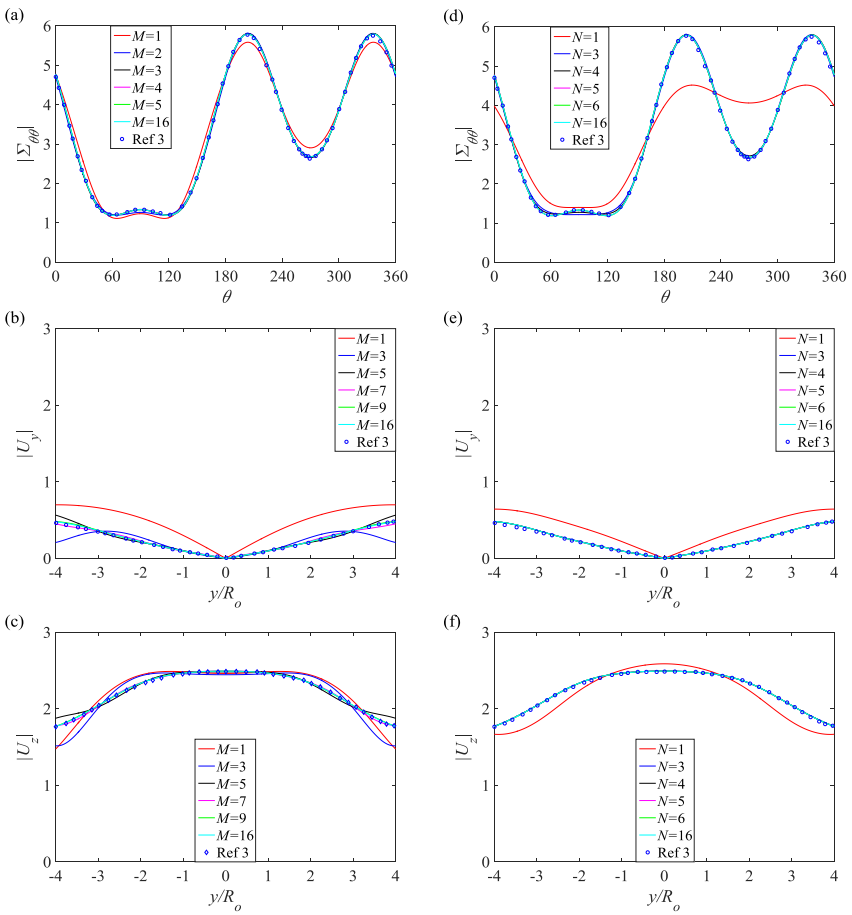


**Fig. 3** Two-dimensional case convergence tests and validations: (a-c) Modes $M$ for the secondary reflected waves with $N=6$; (d-f) Modes $N$ for the directly scattered waves by the cavity with $M=9$; (a), (d) Normalized hoop stress at $r=R_o$; (b), (e) Normalized horizontal displacement at $z=0$; (c), (f) Normalized vertical displacement at $z=0$; $\theta_v=0$, $\theta_h=90$, $h/R_o=5$, $\varpi=0.5$

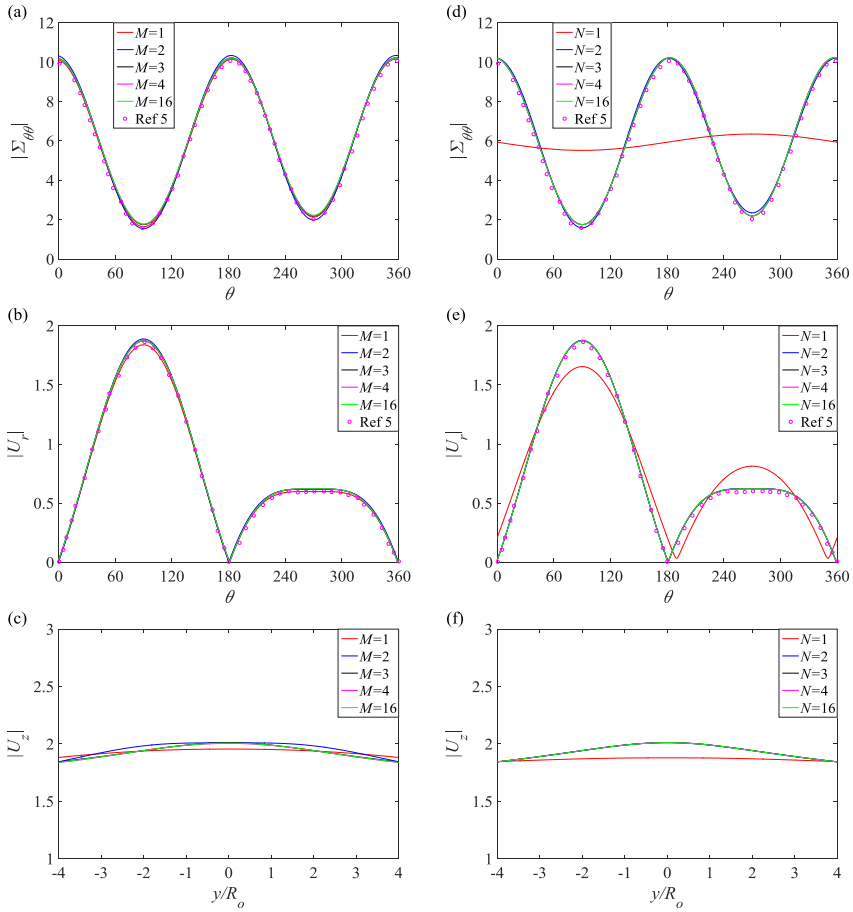


**Fig. 4** Three-dimensional case convergence tests and validations (a-c) Modes $M$ for the secondary reflected waves with $N=3$; (d-e) Modes $N$ for the directly scattered waves by the cavity with $M=3$; (a), (d) Normalized hoop stress at $r=R_C$; (b), (e) Normalized radial displacement at $r=R_O$; (c), (f) Normalized vertical displacement at $z=0$; $\theta_v=30$, $\theta_h=0$, $h=5R_i=4.545R_o$, $\varpi=0.105$

Fig. 5 (a) shows the hoop stresses at the soil-tunnel interface from the soil side ($r=R_O$) for the two- and three-dimensional cases with cavity and tunnel. Fig. 5 (b) shows the hoop stresses on the centreline of the tunnel ($r=R_C$) for the two- and three-dimensional cases with tunnel. It is observed that the distributions of the hoop stress in each case are similar, though the magnitudes are quite different. Additionally, the hoop stresses in the two-dimensional cases are larger than those in the three-dimensional cases, and the hoop stresses in the cavity cases are larger than those in the tunnel cases. Furthermore, the hoop stress in the three-dimensional cavity case is greater than that in the two-dimensional tunnel case. The hoop stress at the soil-tunnel interface from the soil side is reduced mainly due to the fact that

the waves also propagate in the longitudinal direction of the structure and also due to the presence of the scattered waves in the tunnel, both taking away energy. For the two- and three-dimensional cases, we observe that the hoop stress on the centre line of the tunnel are larger than that at the soil-tunnel interface from the soil side.

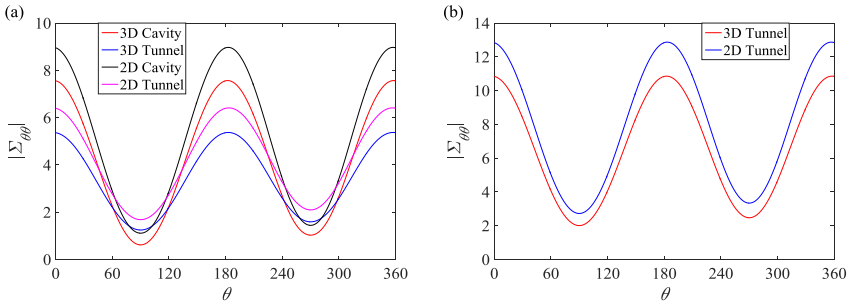


**Fig. 5** (a) Normalized hoop stress at $r = R_O$; (b) Normalized hoop stress at $r = R_C$; $N = M = 4$, $h = 5R_O$, $\varpi = 0.105$, 2D case ($\theta_v = 0$, $\theta_h = 90$), 3D case ($\theta_v = 30$, $\theta_h = 0$)

Figs. 6 (a-c) and (d-f) show the motions at $r = R_O$ and $z = 0$ for all cases. We observe the same trend for the normal and tangential displacements at $r = R_O$ and vertical displacements at $z = 0$ as for the hoop stress, but the motions in the two-dimensional tunnel case are greater than those in the three-dimensional cavity case. The horizontal displacements at $z = 0$ are smaller compared with the vertical and $x$ axial displacements. That is because the horizontal motions are barely excited under nearly vertically incident wave.

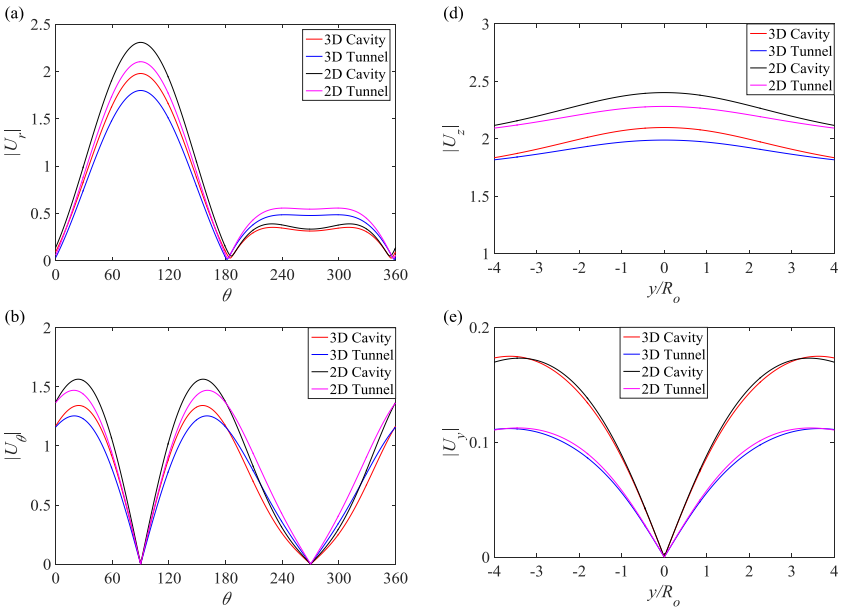

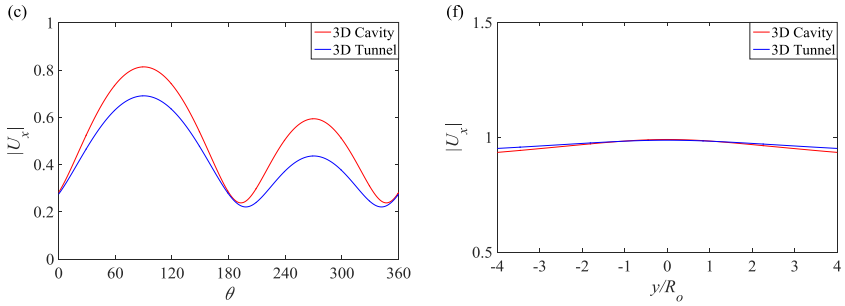


**Fig. 6** (a-c) Normalized displacements at $r = R_O$; (d-f) Normalized displacements at $z = 0$; $N = M = 4$, $h = 5R_O$, $\varpi = 0.105$, 2D case ($\theta_v = 0$, $\theta_h = 90$), 3D case ($\theta_v = 30$, $\theta_h = 0$)

## 8. Conclusions

A semi-analytical method was presented for the theoretical analysis of two- and three-dimensional seismic responses of a tunnel embedded in an elastic half-space. The complex variable theory, conformal mapping and the spirit of the image technique were applied to solve the problem. The results obtained using the proposed method for both the two- and three- dimensional cases are in good agreement with those obtained by the other methods, which confirms the accuracy of the proposed method. This paper also evaluates the contribution of the wave field directely scattered by the tunnel and the secondary reflected wave field on the satisfaction of the bounary conditions at the half-space surface and at the soil-tunnel interface. It was shown that the waves directly scattered by the tunnel affect the satisfaction of the boundary conditions and responses at the soil-tunnel interface and barely affect those at the half-space surface. Correspondingly, the secondary reflected waves contribute to the satisfaction of the boundary conditions and responses at the half-space surface and barely contribute to those at the soil-tunnel interface. The investigation of the effects of the dimension and the presence of the tunnel on the system response showed that the additional dimension and the presence of the tunnel reduce the hoop stress at the interface form the soil side. If the design of the underground structure is based on a simple two-dimensional cavity model, it would be a conservative design according to our analysis.

The advantages of the proposed method are as follows. First, it is a semi-analytical solution of the problem which reveals that the directly scattered waves and the secondary reflected waves contribute to the system response differently. Secondly, the traction-free boundary conditions are in principle satisfied at the entire half-space surface without truncating at a certain distance from the tunnel. Thirdly, when compared with numerical methods, the computational time is significantly reduced. Furthermore, the solution in the half-space can be combined with a finite-element representation for embedded structures that are complex in shape.

The disadvantage of the proposed method is that the matrix used to determine

the unknown coefficients of the cylindrical waves becomes ill-conditioned when we consider very high-frequency excitation, very large shear modulus ratio of the tunnel to the medium and very small depth ratio of the embedded depth to the radius of the tunnel. Correspondingly, the far-field boundary conditions at the half-space surface cannot be satisfied exactly due to some numerical issues, even though the boundary conditions are supposed to be satisfied exactly. Other techniques or a hybrid method will be investigated in the future to overcome this problem.

## Acknowledgements

The study is financially supported by the China Scholarship Council.

## References

[1] Ariman, J., Muleski, G. E. (1981). A review of the response of buried pipelines under seismic excitations, Earthquake Engineering and Structure Dynamics, 9: 133-151.

[2] Stamos, A. A., Beskos, D. E. (1995). Dynamic analysis of large 3-D underground structures by the BEM, Earthquake Engineering and Structural Dynamics, 24: 917-934.

[3] Luco J. E., De Barros F. C. P. (1994). Dynamic displacements and stresses in the vicinity of a cylindrical cavity embedded in a half-space, Earthquake Engineering and Structural Dynamics, 23: 321-340.

[4] Luco, J. E., De Barros, F. C. P. (1994). Seismic response of a cylindrical shell embedded in a layered viscoelastic half-space. I: Formulation, Earthquake Engineering and Structural Dynamics, 23: 553-567.

[5] De Barros, F. C. P., Luco, J. E. (1994). Seismic response of a cylindrical shell embedded in a layered viscoelastic half-space. II: Validation and numerical results. Earthquake Engineering and Structural Dynamics, 23: 569-580.

[6] Wong, K. C., Datta, S. K., Shah, A. H. (1986). Three-dimensional motion of buried pipeline. II: Numerical results, Journal of Engineering Mechanics, 112: 1338-1345.

[7] Liu, S. W., Datta, S. K., Khair, K. R. (1991). Three dimensional dynamics of pipelines buried in backfilled trenches due to oblique incidence of body wave, Soil Dynamics and Earthquake Engineering, 10: 182-191.

[8] Data S. K., Shah A. H., Wong K. C. (1984). Dynamic stresses and displacements in buried pipe, Journal of Engineering Mechanics, 110 (10): 1451-4166.

[9] Balendra T., Thambiratnam D. P., Koh C. G., Lee S. -L. (1984). Dynamic response of twin circular tunnels due to incident SH-waves, Earthquake Engineering and Structural Dynamics, 12: 181-201.

[10] Liu, Q., Zhao, M., Wang, L. (2013). Scattering of plane P, SV or Rayleigh waves by a shallow lined tunnel in an elastic half space, Soil Dynamics and Earthquake Engineering, 49: 52-63.
[11] Liu, Q., Zhao, M., Zhang, C. (2014). Antiplane scattering of SH waves by a circular cavity in an exponentially graded half space, International Journal of Engineering Science, 78: 61-72.
[12] Gregory R. D. (1967). An expansion theorem applicable to problems of wave propagation in an elastic half-space containing a cavity, Mathematical Proceedings of the Cambridge Philosophical Society, 63 (4): 1341-1367.
[13] Kausel E. (2006). Fundamental Solution in Elastodynamics: A Compendium, Cambridge University Press, UK.
[14] Aki K., Richards P. (2002). Quantative Seismology, Univeristy Science Books, Sausalito, California.
[15] Graff, K. F. (1975). Wave Motion in Elastic Solids, Courier Corporation.
[16] Verruijt A. (1998). Deformations of an elastic half plane with a circular cavity, International Journal of Solids and Structures, 35: 2795-2804.
[17] Muskhelishvili NI. (1966). Some Basic Problems of the Mathematical Theory of Elasticity, Cambridge University Press.
[18] Liu D. K., Gai B., Tao G. (1982). Application of the method of complex functions to dynamic stress concentrations, Wave Motion, 4: 293-304.